

# RecConv: Efficient Recursive Convolutions for Multi-Frequency Representations

Mingshu Zhao<sup>1</sup> Yi Luo<sup>1</sup> Yong Ouyang<sup>1,2</sup>

<sup>1</sup>Sichuan Energy Internet Research Institute, Tsinghua University

<sup>2</sup>Chengdu Qingrong Shentong Technology

zhaomingshu@tsinghua-eiri.org luoyi@tsinghua-eiri.org ouyangyong@deepsensing.cn

## Abstract

Recent advances in vision transformers (ViTs) have demonstrated the advantage of global modeling capabilities, prompting widespread integration of large-kernel convolutions for enlarging the effective receptive field (ERF). However, the quadratic scaling of parameter count and computational complexity (FLOPs) with respect to kernel size poses significant efficiency and optimization challenges. This paper introduces RecConv, a recursive decomposition strategy that efficiently constructs multi-frequency representations using small-kernel convolutions. RecConv establishes a linear relationship between parameter growth and decomposing levels which determines the effective kernel size  $k \times 2^\ell$  for a base kernel  $k$  and  $\ell$  levels of decomposition, while maintaining constant FLOPs regardless of the ERF expansion. Specifically, RecConv achieves a parameter expansion of only  $\ell + 2$  times and a maximum FLOPs increase of  $5/3$  times, compared to the exponential growth ( $4^\ell$ ) of standard and depthwise convolutions. RecNeXt-M3 outperforms RepViT-M1.1 by  $1.9 AP^{box}$  on COCO with similar FLOPs. This innovation provides a promising avenue towards designing efficient and compact networks across various modalities. Codes and models can be found at <https://github.com/suous/RecNeXt>.

## 1. Introduction

Convolutional Neural Networks (CNNs) [18, 27, 28, 49] have been foundational in computer vision for years, exploiting their intrinsic locality and translation equivariance [12]. Nonetheless, the recent emergence of vision transformers (ViTs) has demonstrated that establishing global context through self-attention mechanisms can lead to superior performance on various computer vision benchmarks [2, 12, 73]. Following the success of ViTs, extensive research has validated the effectiveness of large kernel convolutions in augmenting model capabilities through expanded receptive fields. ConvNeXt [38] and RepLkNet [9] achieved performance comparable or superior to Swin

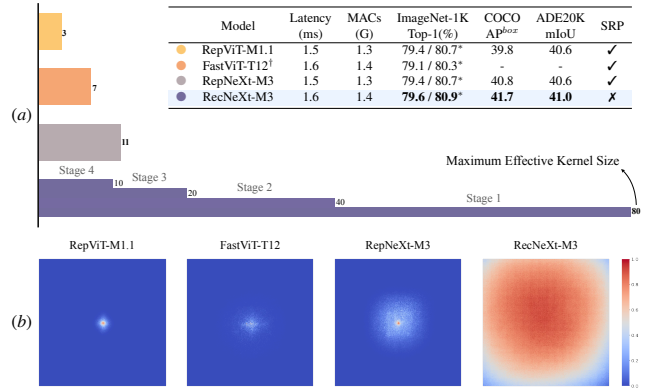


Figure 1. **Effective Receptive Field (ERF) and Model Performance.** (a) Comparison of effective kernel sizes and performance metrics among RecNeXt and prominent lightweight models. Top-1 accuracy is evaluated on ImageNet-1K and the latency is assessed using an iPhone 13 running iOS 18, where all models are formatted into *mlmodel*. “†” denotes pretraining at  $256 \times 256$  resolution and “\*” indicates pretraining with hard knowledge distillation. (b) The effective receptive fields of RepViT [64], FastViT [60], RepNeXt [72], and RecNeXt, where all models are pretrained with hard knowledge distillation. RecNeXt exhibits the broadest ERF, maintaining competitive latency and superior performance without reliance on structural reparameterization (SRP).

Transformers [37] when aligned with contemporary design paradigms. SLaK [36] and PeLK [3] explored kernels beyond  $51 \times 51$  and  $101 \times 101$  through dynamic sparsity and parameter sharing. Moreover, large-kernel CNNs have shown superiority as teachers in knowledge distillation for compact CNNs [24].

Although large-kernel convolutions provide superior performance, the quadratic scaling of parameter count and computational complexity relative to kernel size presents substantial efficiency challenges and optimization difficulties, restricting their practical deployment on resource-constrained devices. Consequently, small-kernel convolutions are still preferred [34, 51, 64, 65] in such scenarios considering their optimized algorithms and compact weights. Recent studies have explored large-kernel convolutions in resource-constrained environments. FastViT [60],

StarNet [39], and EfficientMod [40] employed  $7 \times 7$  depthwise convolutions to capture long-range dependencies. EdgeNeXt [41] introduced adaptive kernel mechanisms for multi-level feature extraction. MobileMamba [17] enhanced multi-scale representations through a multi-receptive field feature interaction module. RepNeXt [72] employed multi-branch efficient operations to replace the  $11 \times 11$  depthwise convolution. However, the application of even larger convolution kernels in resource-constrained settings remains unexplored.

OctConv [5] leveraged octave convolutions to enable multi-frequency feature representation. WTConv [13] incorporated small-kernel convolutions with cascade wavelet decomposition to obtain global receptive fields. While effective, their implementation requires substantial amount of parameters and resource-intensive operations. Motivated by the multi-frequency response observed in OctConv and WTConv, we propose RecConv — a recursively decomposed multi-frequency convolution optimized for resource-constrained mobile vision applications. Based on RecConv, we introduce RecNeXt, a simple yet effective vision backbone that delivers competitive efficiency with superior performance. Our contributions can be concluded as follows:

- Inspired by WTConv [13], we develop a recursive decomposition strategy to generate multi-frequency representations. This approach establishes a linear relationship between parameter growth and decomposing levels, while maintaining constant FLOPs, making it highly adaptable for designing efficient networks with large receptive fields across diverse modalities.
- Following this design principle, we construct RecConv as a plug-and-play module that can be seamlessly integrated into existing computer vision architectures.
- Leveraging RecConv, we introduce RecNeXt, an efficient and effective vision backbone equipped with large receptive fields and optimized towards resource-constrained mobile vision applications.
- Extensive experiments across various vision benchmarks demonstrate the superiority of RecNeXt over current leading approaches without relying on neural architecture search (NAS) or structural reparameterization (SRP).

## 2. Related Work

**Large Kernel CNNs:** Large kernels have been explored in early CNNs [27, 53], but fell out of favor after VGG [52]. ConvNeXt [38] and ConvMixer [59] embraced contemporary design philosophy with large-kernel depthwise convolutions, replicating the global perspective of ViTs [12] and MLP-Mixers [58]. MogaNet [30] incorporated multi-scale spatial aggregation blocks with dilated convolutions to capture discriminative features. SKNet [31] and LSKNet [33] employed multi-branch selective mechanisms along the channel or spatial dimension. RepLKNet [9] achieved per-

formance comparable to Swin Transformers [37] by expanding kernel size to  $31 \times 31$  with SRP. UniRepLKNet [10] demonstrated the universal applicability of large-kernel designs across various modalities. SLaK [36] improved performance by expanding kernels beyond  $51 \times 51$  using stripe convolutions and dynamic sparsity. PeLK [3] explored kernels up to  $101 \times 101$  in a human-like pattern without performance saturation. GFNet [48] leveraged Fourier transforms to capture long-term spatial dependencies in the frequency domain. WTConv [13] replaced large-kernel convolutions with a set of small-kernel convolutions through wavelet decomposition. Furthermore,  $n \times n$  convolutions are often factorized into sequential or parallel  $1 \times n$  and  $n \times 1$  convolutions for efficiency [15, 46, 54, 55, 69]. Additionally, LargeKernel3D [7] and ModernTCN [11] extended large kernel design to 3D networks and time series analysis.

**Efficient Networks:** Developing efficient networks for resource-constrained vision applications has attracted significant attention [22, 49, 65]. MobileNets [21, 22, 50] proposed depthwise separable convolutions and inverted residual blocks to optimize the efficiency-accuracy trade-off. GhostNet [16], FasterNet [4], and SHViT [70] employed partial channel operations for parameter reduction and computational efficiency. MobileOne [61], FastViT [60], and RepViT [64] utilized structural reparameterization (SRP) to improve feature diversity without increasing the inference latency. MnasNet [57] and EfficientNet [56] leveraged neural architecture search (NAS) to automatically discover efficient architectures. MobileViTs [42, 43, 63], EdgeViTs [45], and EfficientFormers [32, 34] designed hybrid architectures to balance performance and efficiency. MobileFormer [6] and ParC-Net [71] introduced multi-branch feature integration to improve representational capacity. SwiftFormer [51] and LightViT [23] constructed linear attention mechanisms to replace quadratic matrix multiplications. FastViT [60], StarNet [39], and EfficientMod [40] adopted  $7 \times 7$  depthwise convolutions to capture long-range dependencies. EdgeNeXt [41] and RepNeXt [72] introduced multi-branch efficient operations to obtain large-kernel receptive fields. MobileMamba [17] incorporated long-range wavelet transform-enhanced mamba and efficient multi-kernel depthwise convolution to enhance multi-scale perception.

The major perspective of our work is inspired by WTConv [13], while our design focuses on resource-constrained applications. And there are three major differences between WTConv and our proposed method: (1) We adopt a shared and learnable downsampling layer using a depthwise convolution with a stride of 2. (2) We maintain the same channel dimension across different scales for structural consistency and computational efficiency. (3) We use bilinear interpolation as an efficient upsampling operation to reduce parameter count and memory footprint.

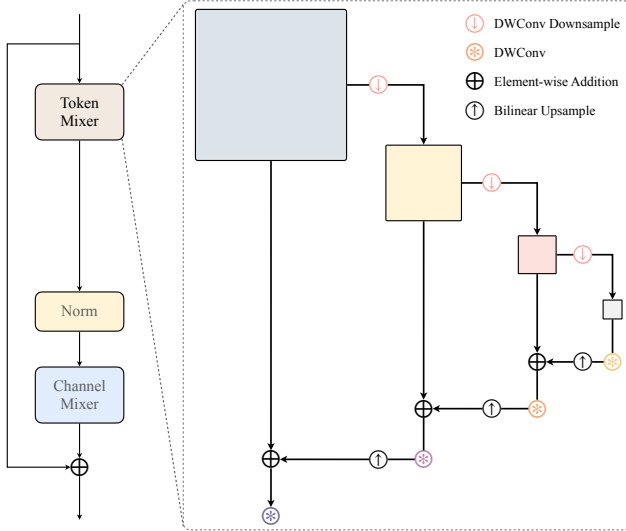


Figure 2. **Recursive Convolution Module (RecConv)**. The left side illustrates a MetaNeXt block abstracted from previous works [38, 68, 69]. The right side highlights the RecConv details, where feature maps are recursively decomposed into multiple spatial scales using a shared depthwise convolutional downsampling layer. Each scale applies a small-kernel depthwise convolution to generate features of varying spatial sizes, which are then up-sampled and aggregated, collectively replicating the large-kernel receptive field while preserving computational and parameter efficiency. This design strategy accommodates various functions and can be extended to other modalities.

### 3. Method

#### 3.1. Overall Architecture

The RecNeXt architecture builds upon RepViT [64] and RepNeXt [72], adhering to the four-stage framework of conventional CNNs [18] and hierarchical ViTs [37]. Starting with two  $3 \times 3$  convolutions with a stride of 2 [34, 64, 67], progressively enhancing semantic representations while reducing spatial dimensions. The micro-blocks adopt the MetaNeXt design [38, 69], incorporating a *token mixer* for spatial feature extraction, a *channel mixer* for visual semantic interaction, a normalization layer [25] for training stability, and a shortcut connection [18] to facilitate smoother optimization [29].

$$Y = X + \text{ChannelMixer}(\text{Norm}(\text{TokenMixer}(X))), \quad (1)$$

where  $X, Y \in \mathbb{R}^{B \times C \times H \times W}$  with  $B$  represents batch size,  $C$  denotes channel number, and  $H$  and  $W$  indicate image height and width, respectively.  $\text{Norm}(\cdot)$  denotes the Batch Normalization (BN) layer [25], which can be fused into the previous convolution layer.  $\text{TokenMixer}(\cdot)$  implements the RecConv and  $\text{ChannelMixer}(X) = \text{Conv}_{1 \times 1, \downarrow}(\sigma(\text{Conv}_{1 \times 1, \uparrow}(X)))$  is a channel MLP module comprising two fully-connected layers with a GELU [20] activate function  $\sigma$  in between, resembling the feed-forward

#### Algorithm 1 RecConv in a PyTorch-like style

```

class RecConv(Module):
    def __init__(self, ic, ks=5, level=1):
        super().__init__()
        self.level = level
        kwargs = {
            'in_channels': ic,
            'out_channels': ic,
            'kernel_size': ks,
            'padding': ks // 2,
            'groups': ic
        }
        # downsample with shared parameters
        self.down = Conv(stride=2, **kwargs)
        # convolutions on different levels
        self.conv = [Conv(**kwargs)] * (level+1)

    def forward(self, x):
        i, fs = x, []
        for _ in range(self.level):
            x, s = self.down(x), x.shape[2:]
            fs.append((x, s))

        x = 0
        for c, (f, s) in zip(self.conv, reversed(fs)):
            x = interpolate(c(f + x), size=s)
        return self.conv[self.level](i + x)

```

network in a Transformer [62].  $\text{Conv}_{1 \times 1, \uparrow}$  and  $\text{Conv}_{1 \times 1, \downarrow}$  stand for  $1 \times 1$  pointwise convolutions for expanding and squeezing feature maps, respectively.

The downsampling layer between each stage is a modified version of the MetaNeXt block [38, 69], where the shortcut connection bypasses the *channel mixer*.

$$\begin{aligned} \hat{X} &= \text{Norm}(\text{TokenMixer}(X)), \\ Y &= \hat{X} + \text{ChannelMixer}(\hat{X}), \end{aligned} \quad (2)$$

where  $\hat{X}, Y \in \mathbb{R}^{B \times 2C \times H/2 \times W/2}$ .  $\text{TokenMixer}(\cdot)$  is a  $7 \times 7$  depthwise convolution with stride 2 for downsampling.

#### 3.2. Recursive Convolution

The right side of Figure 2 spotlights the RecConv details, where initial feature maps are recursively decomposed into multiple spatial scales via a shared depthwise convolutional downsampling layer. Each scale employs a small-kernel depthwise convolution to extract features at varying spatial resolutions, which are then progressively fused back into the original feature map using bilinear upsampling and element-wise addition for simplicity. This efficient and recursive design enables the model to encapsulate multi-frequency representations within each block, effectively replicating the receptive field of large-kernel convolutions without the associated parameter inflation and computational overhead. Furthermore, this flexible and modular design philosophy is compatible with diverse operators, and can be seamlessly integrated into existing vision architectures or extended to other modalities.

Specifically, as demonstrated in Algorithm 1 and Equation 3, feature maps of level  $\ell$  are produced by the previous level  $\ell - 1$  using a depthwise convolution with a stride of

Table 1. **Classification performance on ImgeNet-1K.** Following [32, 64], latency is measured on an iPhone 13 with models compiled by Core ML Tools. Similar to [14], throughput is tested on an Nvidia RTX3090 GPU with maximum power-of-two batch size that fits in memory. “†” denotes the evaluation image size is 256.

Model	Type	Params (M)	MACs (G)	Latency ↓ (ms)	Throughput ↑ (im/s)	Top1 ↑ (%)	Auxiliary	
							NAS	SRP
MobileViG-Ti [44]	CNN-GNN	5.2	0.7	1.4	4337	75.7	✗	✗
SwiftFormer-XS [51]	Hybrid	3.5	0.6	1.5	4304	75.7	✗	✗
EfficientFormerV2-S0 [34]	Hybrid	3.5	0.4	1.4	1274	75.7	✓	✗
FastViT-T8† [60]	Hybrid	3.6	0.7	1.3	3909	76.7	✗	✓
RepViT-M0.9 [64]	CONV	5.1	0.8	1.3	4817	78.7	✗	✓
RepNeXt-M1 [72]	CONV	4.8	0.8	1.3	3885	78.8	✗	✓
EfficientFormerV2-S1 [34]	Hybrid	6.1	0.7	1.6	1153	79.0	✓	✗
RepViT-M1.0 [64]	CONV	6.8	1.1	1.4	3910	80.0	✗	✓
RepNeXt-M2 [72]	CONV	6.5	1.1	1.4	3198	80.1	✗	✓
<b>RecNeXt-M1</b>	CONV	5.2	0.9	1.4	384	<b>79.2</b>	✗	✗
<b>RecNeXt-M2</b>	CONV	6.8	1.2	1.5	325	<b>80.3</b>	✗	✗
MobileViG-S [44]	CNN-GNN	7.2	1.0	1.6	2985	78.2	✗	✗
SwiftFormer-S [51]	Hybrid	6.1	1.0	1.8	3376	78.5	✗	✗
EfficientFormer-L1 [32]	Hybrid	12.3	1.3	1.8	3360	79.2	✓	✗
FastViT-T12† [60]	Hybrid	6.8	1.4	1.8	3182	80.3	✗	✓
RepViT-M1.1 [64]	CONV	8.2	1.3	1.5	3604	80.7	✗	✓
RepNeXt-M3 [72]	CONV	7.8	1.3	1.5	2903	80.7	✗	✓
<b>RecNeXt-M3</b>	CONV	8.2	1.4	1.6	314	<b>80.9</b>	✗	✗
MobileViG-M [44]	CNN-GNN	14.0	1.5	2.0	2491	80.6	✗	✗
FastViT-S12† [60]	Hybrid	8.8	1.8	2.0	2313	80.9	✗	✓
SwiftFormer-L1 [51]	Hybrid	12.1	1.6	2.2	2576	80.9	✗	✗
EfficientFormerV2-S2 [34]	Hybrid	12.6	1.3	2.3	611	81.6	✓	✗
FastViT-SA12† [60]	Hybrid	10.9	1.9	2.3	2181	81.9	✗	✓
RepViT-M1.5 [64]	CONV	14.0	2.3	1.9	2151	82.3	✗	✓
RepNeXt-M4 [72]	CONV	13.3	2.3	1.9	1745	82.3	✗	✓
<b>RecNeXt-M4</b>	CONV	14.1	2.4	2.4	169	<b>82.5</b>	✗	✗
EfficientFormer-L3 [32]	Hybrid	31.3	3.9	3.4	1422	82.4	✓	✗
MobileViG-B [44]	CNN-GNN	26.7	2.8	3.5	1446	82.6	✗	✗
SwiftFormer-L3 [51]	Hybrid	28.5	4.0	3.4	1474	83.0	✗	✗
EfficientFormer-L7 [32]	Hybrid	82.1	10.2	7.1	619	83.3	✓	✗
EfficientFormerV2-L [34]	Hybrid	26.1	2.6	3.8	399	83.3	✓	✗
RepViT-M2.3 [64]	CONV	22.9	4.5	2.8	1184	83.3	✗	✓
FastViT-SA24† [60]	Hybrid	20.6	3.8	3.4	1128	<b>83.4</b>	✗	✓
RepNeXt-M5 [72]	CONV	21.7	4.5	2.8	978	83.3	✗	✓
<b>RecNeXt-M5</b>	CONV	22.9	4.7	3.4	104	83.3	✗	✗

2. This process then generates new feature maps at level  $\ell + 1$  using the same downsampling operation. Higher-level feature maps are processed through depthwise convolutions and then progressively integrated back into previous levels through bilinear interpolation and element-wise addition. This recursive design maintains parameter efficiency as decomposition levels increase by reusing the downsampling layer and employing a parameter-free upsampling operation across all decomposition levels.

$$\begin{aligned}
 X_\ell &= \text{DWConv}_{k \times k, \downarrow}(X_{\ell-1}), \\
 X_\ell &= X_\ell + \text{Interp}_\uparrow \left( \text{DWConv}_{k \times k}^{(\ell+1)}(X_{\ell+1}) \right), \quad (3)
 \end{aligned}$$

where  $X_{\ell-1} \in \mathbb{R}^{B \times C \times 2h \times 2w}$ ,  $X_\ell \in \mathbb{R}^{B \times C \times h \times w}$ , and  $X_{\ell+1} \in \mathbb{R}^{B \times C \times \frac{h}{2} \times \frac{w}{2}}$  represent feature maps at levels  $\ell - 1$ ,  $\ell$ , and  $\ell + 1$ , respectively.  $\text{DWConv}_{k \times k, \downarrow}$  indi-

cates the shared-weight depthwise convolution with a kernel size of  $k \times k$  and a stride of 2, while  $\text{DWConv}_{k \times k}^{(\ell+1)}$  denotes the depthwise convolution with a kernel size of  $k \times k$  at level  $\ell + 1$ .  $\text{Interp}_\uparrow$  stands for the bilinear interpolation upsampling operation. Features at different scales are progressively fused back into the original feature map, effectively replicating multi-frequency representations with large-kernel receptive fields.

Table 2 illustrates that to achieve a larger effective kernel size of  $k \times 2^\ell$ , both standard and depthwise convolutions require exponential growth in parameters and FLOPs with respect to the decomposition level  $\ell$ . In contrast, RecConv exhibits only linear growth in parameters while maintaining constant FLOPs. Specifically, RecConv consists of a shared-weight depthwise convolutional downsampling module and  $\ell + 1$  depthwise convolution layers, which pri-



Table 2. **Complexity of different types of convolution.** The measurement is streamlined by focusing on convolution operations, with the assumption of consistent input and output channels, and excluding the bias term.  $k$ ,  $C$ ,  $H$  and  $W$  denote the base kernel size, channel number, image height and width, respectively. And  $\ell$  represents the number of decomposition levels that determine the effective kernel size, which is  $k \times 2^\ell$ .

Convolution	Parameters	FLOPs
Standard	$k^2 C \times (4^\ell C)$	$k^2 CHW \times (4^\ell C)$
Depthwise	$k^2 C \times (4^\ell)$	$k^2 CHW \times (4^\ell)$
RecConv	$k^2 C \times (\ell + 2)$	$k^2 CHW \times (5/3)$

marily contribute to the parameter count and FLOPs. The parameter count remains consistent across the downsampling layer and depthwise convolutions at each level, growing by a factor of  $\ell + 2$  compared to the base kernel. FLOPs can be regarded as a series of geometric progression, decreasing exponentially as the levels increase, as demonstrated in Equation 4. Consequently, RecConv achieves linear parameter growth and nearly constant FLOPs proportional to the decomposition level, making it an efficient solution for attaining large receptive fields in resource-constrained scenarios.

$$1 + 2 \sum_{n=1}^{\ell} \frac{1}{4^n} < \sum_{n=0}^{\infty} 2 \cdot \left(\frac{1}{4}\right)^n - 1 = \frac{5}{3} \quad (4)$$

In addition, our RecConv embodies a versatile design philosophy that accommodates different operators and dimensions. For instance, the shared downsampling layer can be substituted with a sequence of channel-wise chunking operations followed by depthwise convolutions; depthwise convolutions at each level can be replaced by efficient attention mechanisms; bilinear upsampling operations can be converted to transposed convolutions; and element-wise addition can be reconfigured as channel-wise concatenation.

## 4. Experiments

We demonstrate the versatility and efficacy of RecNeXt across multiple vision tasks: classification on ImageNet-1K [8], object detection and instance segmentation on MS-COCO 2017 [35], and semantic segmentation on ADE20K [74]. Following prior works [32, 34, 43, 61, 64, 72], we export the model using Core ML Tools [1] and assess its latency on an iPhone 13 (iOS 18) using the Xcode performance tool. Additionally, we measure throughput on an Nvidia RTX3090 GPU with the maximum power-of-two batch size that can be accommodated in memory.

### 4.1. Image Classification

**Implementation details.** We perform image classification on ImageNet-1K using a standard image resolution of

Table 3. Results without distillation on ImageNet-1K, where “†” denotes the evaluation image size is 256.

Model	Latency (ms)	Params (M)	Top-1 (%)	Auxiliary NAS	SRP
EfficientFormerV2-S0 [34]	1.4	3.5	73.7	✓	✗
FastViT-T8† [60]	1.3	3.6	75.6	✗	✓
MobileOne-S1 [61]	1.2	4.8	75.9	✗	✓
RepViT-M0.9 [64]	1.3	5.1	77.4	✗	✓
RepNeXt-M1 [72]	1.3	4.8	77.5	✗	✓
RepViT-M1.0 [64]	1.4	6.8	78.6	✗	✓
RepNeXt-M2 [72]	1.4	6.5	78.9	✗	✓
<b>RecNeXt-M1</b>	1.4	5.2	<b>78.0</b>	✗	✗
<b>RecNeXt-M2</b>	1.5	6.8	<b>79.2</b>	✗	✗
MobileOne-S2 [61]	1.5	7.8	77.4	✗	✓
EfficientFormerV2-S1 [34]	1.6	6.1	77.9	✓	✗
MobileOne-S3 [61]	1.7	10.1	78.1	✗	✓
FastViT-T12† [60]	1.8	6.8	79.1	✗	✓
RepViT-M1.1 [64]	1.5	8.2	79.4	✗	✓
RepNeXt-M3 [72]	1.5	7.8	79.4	✗	✓
<b>RecNeXt-M3</b>	1.6	8.2	<b>79.6</b>	✗	✗
MobileOne-S4 [61]	2.2	14.8	79.4	✗	✓
FastViT-S12† [60]	2.0	8.8	79.8	✗	✓
PoolFormer-S24 [68]	3.2	21.0	80.3	✗	✗
EfficientFormerV2-S2 [34]	2.3	12.6	80.4	✓	✗
FastViT-SA12† [60]	2.3	10.9	80.6	✗	✓
RepViT-M1.5 [64]	1.9	14.0	81.2	✗	✓
RepNeXt-M4 [72]	1.9	13.3	<b>81.2</b>	✗	✓
<b>RecNeXt-M4</b>	2.4	14.1	81.1	✗	✗
PoolFormer-S36 [68]	4.3	31.0	81.4	✗	✗
RepViT-M2.3 [64]	2.8	22.9	82.5	✗	✓
FastViT-SA24† [60]	3.4	20.6	<b>82.6</b>	✗	✓
RepNeXt-M5 [72]	2.8	21.7	82.4	✗	✓
<b>RecNeXt-M5</b>	3.4	22.9	81.6	✗	✗

224×224 for both training and evaluation. This dataset consists of 1.3M training, 50k validation, and 100k test images across 1000 categories. All models are trained from scratch for 300 epochs following the training protocol in [34, 60, 64, 72]. For fair comparisons, we employ the RegNetY-16GF [47] model (top-1 accuracy 82.9%) as the teacher model for hard knowledge distillation. Latency is measured on an iPhone 13 with models compiled via Core ML Tools at a batch size of 1. Performance with and without distillation is reported in Table 1 and 3, respectively.

**Results with knowledge distillation.** As demonstrated in Table 1, RecNeXt consistently delivers superior performance and competitive latency across various model sizes without requiring additional training auxiliaries. Notably, smaller RecNeXt models outperform their RepNeXt counterparts by 0.2% in top-1 accuracy while maintaining comparable latency and FLOPs. RecNeXt-M5 matches the top-1 accuracy (83.3%) of EfficientFormerV2-L with fewer parameters and lower latency. Without leveraging structural reparameterization (SRP) or neural architecture search (NAS), the RecNeXt series consistently surpasses SwiftFormer in top-1 accuracy with similar computational complexity. However, RecNeXt encounters challenges with

Table 4. **Object detection and instance segmentation** were evaluated using Mask R-CNN on MS-COCO 2017. **Semantic segmentation** results were obtained on ADE20K. Backbone latencies were measured on an iPhone 13 with  $512 \times 512$  image crops using Core ML Tools. Models marked with “†” were initialized with weights pretrained for 450 epochs on ImageNet-1K.

Backbone	Latency ↓ (ms)	Object Detection			Instance Segmentation			Semantic
		$AP^{box}$	$AP_{50}^{box}$	$AP_{75}^{box}$	$AP^{mask}$	$AP_{50}^{mask}$	$AP_{75}^{mask}$	mIoU
ResNet18 [18]	3.8	34.0	54.0	36.7	31.2	51.0	32.7	32.9
PoolFormer-S12 [68]	6.2	37.3	59.0	40.1	34.6	55.8	36.9	37.2
FastViT-SA12 [60]	7.6	38.9	60.5	42.2	35.9	57.6	38.1	38.0
RepViT-M1.1 [64]	4.1	39.8	61.9	43.5	37.2	58.8	40.1	40.6
RepNeXt-M3 [72]	4.3	40.8	62.4	44.7	37.8	59.5	40.6	40.6
RecNeXt-M3	5.2	<b>41.7</b>	<b>63.4</b>	<b>45.4</b>	<b>38.6</b>	<b>60.5</b>	<b>41.4</b>	<b>41.0</b>
PoolFormer-S24 [68]	10.5	40.1	62.2	43.4	37.0	59.1	39.6	40.3
PVT-Small [66]	26.2	40.4	62.9	43.8	37.8	60.1	40.3	39.8
SwiftFormer-L1 [51]	6.2	41.2	63.2	44.8	38.1	60.2	40.7	41.4
RepViT-M1.5 [64]	5.7	41.6	63.2	45.3	38.6	60.5	41.5	43.6
FastViT-SA24 [60]	12.2	42.0	63.5	45.8	38.0	60.5	40.5	41.0
RepNeXt-M4 [72]	6.1	42.9	64.4	47.2	39.1	61.7	41.7	43.3
RecNeXt-M4	7.6	<b>43.5</b>	<b>64.9</b>	<b>47.7</b>	<b>39.7</b>	<b>62.1</b>	<b>42.4</b>	<b>43.6</b>
SwiftFormer-L3 [51]	10.4	42.7	64.4	46.7	39.1	61.7	41.8	43.9
FastViT-SA36 [60]	16.2	43.8	65.1	47.9	39.4	62.0	42.3	42.9
RepViT-M2.3† [64]	9.0	44.6	66.1	48.8	<b>40.8</b>	<b>63.6</b>	<b>43.9</b>	<b>46.1</b>
RepNeXt-M5 [72]	9.3	<b>44.7</b>	66.0	<b>49.2</b>	40.7	63.5	43.6	45.0
RecNeXt-M5	12.4	44.6	<b>66.3</b>	49.0	40.6	63.5	43.5	46.0

throughput due to the extensive employment of bilinear up-sample operations, which are less friendly to GPU acceleration. This deficiency can be alleviated by leveraging transposed depthwise convolutions at the cost of increased computational complexity and parameter count.

**Results without knowledge distillation.** Table 3 illustrates that RecNeXt maintains strong performance across various model scales. RecNeXt-M1 achieves a top-1 accuracy of 78.0% with a latency of 1.4 ms and 5.2M parameters, outperforming prior lightweight models such as RepViT-M0.9 (77.4%) and RepNeXt-M1 (77.5%) at comparable latencies. RecNeXt-M2 further improves to 79.2% accuracy with 6.8M parameters and 1.5 ms latency, surpassing RepViT-M1.0 (78.6%) and RepNeXt-M2 (78.9%) under similar resource constraints. For higher-capacity models, RecNeXt-M3 achieves a top-1 accuracy of 79.6%, exceeding other leading models without relying on structural reparameterization (SRP) and neural architecture search (NAS). However, larger models like RecNeXt-M4 and RecNeXt-M5 exhibit performance saturation alongside increased latency, with RecNeXt-M5 plateaus at 81.6% top-1 accuracy but with a latency of 3.4ms (0.6ms higher than RepNext-M5). Although RecNeXt-M5 experiences performance degradation, it still outperforms PoolFormer-S36 (81.4%) under the same training protocol, with fewer parameters and lower latency. Additionally, incorporating SRP or advanced

operators could potentially mitigate this limitation.

## 4.2. Downstream Tasks

**Object Detection and Instance Segmentation.** We evaluate RecNeXt’s transfer ability on object detection and instance segmentation tasks. Following [34], we integrate RecNeXt into the Mask-RCNN framework [19] and conduct experiments on the MS-COCO 2017 dataset [35], presenting metrics of  $AP^{box}$  and  $AP^{mask}$ . As shown in Table 4, RecNeXt demonstrates superior performance in terms of  $AP^{box}$  and  $AP^{mask}$  while maintaining competitive latency. For instance, RecNeXt-M3 achieves a notable  $AP^{box}$  of 41.7 and  $AP^{mask}$  of 38.6 while maintaining a latency of 5.2ms, offering an optimal trade-off between speed and precision. RecNeXt-M4 surpasses FastViT-SA24 by 1.5  $AP^{box}$  and 1.7  $AP^{mask}$  with 4ms latency improvement, and increases the  $AP^{box}$  and  $AP^{mask}$  by 0.6 compared to RepNext-M4 with only 0.5ms latency increase. However, RecNeXt-M5 encounters a performance saturation at 44.6  $AP^{box}$  and 40.6  $AP^{mask}$ , albeit with a higher latency of 12.4ms compared to 9.3ms of RepNext-M5.

**Semantic Segmentation.** We perform semantic segmentation experiments on the ADE20K dataset [74], which consists of approximately 20K training images and 2K validation images across 150 categories. Intersection-over-Union (mIoU) is used as the evaluation metric. We followed the

Table 5. **Ablation study conducted under 120 epochs on the ImageNet-1K classification benchmark.** Metrics reported include top-1 accuracy on the validation set, latency on an iPhone 13 running iOS 18, and throughput on a RTX3090 GPU. Experiments were conducted at image resolutions of both 224 and 384 to validate the effectiveness of large receptive fields. “ $\square$ ” represents the simultaneous recursive decomposition in both spatial and channel dimensions. “ $\otimes$ ” indicates the shared downsample operation and bilinear upsample operation are replaced by transposed group convolutions. “ $\ominus$ ” denotes the element-wise addition is replaced by channel-wise concatenation.

Image Size	Levels	Kernel Size	Receptive Field	Params (M)	MACs (G)	Latency (ms)	Throughput (im/s)	Top1 (%)	Upsample Operation
224 × 224	-	3 × 3	[3, 3, 3, 3]	4.80	0.82	1.24	4479	74.64	Bilinear Interpolate
		7 × 7	[7, 7, 7, 7]	4.96	0.87	1.27	3529	75.52	
		11 × 11	[11, 11, 11, 11]	5.26	0.96	1.31	2591	75.41	
	[4, 3, 2, 1]	3 × 3	[48, 24, 12, 6]	4.90	0.83	1.33	389	75.48	
		5 × 5	[80, 40, 20, 10]	5.16	0.87	1.36	384	<b>76.03</b>	
		7 × 7	[112, 56, 28, 14]	5.55	0.92	1.43	374	75.67	
384 × 384	-	3 × 3	[3, 3, 3, 3]	4.80	2.40	2.07	1553	76.35	Bilinear Interpolate
		7 × 7	[7, 7, 7, 7]	4.96	2.55	2.20	1224	77.42	
		11 × 11	[11, 11, 11, 11]	5.26	2.82	2.27	880	78.00	
		3 × 3	[48, 24, 12, 6]	4.90	2.44	2.71	320	77.72	
	[4, 3, 2, 1]	5 × 5	[80, 40, 20, 10]	5.16	2.54	2.79	311	<b>78.11</b>	DWConv Transpose
		7 × 7	[112, 56, 28, 14]	5.55	2.69	2.84	295	78.03	
		3 × 3	[48, 24, 12, 6]	4.97	2.44	2.40	993	77.26	
		5 × 5	[80, 40, 20, 10]	5.31	2.57	2.48	784	77.87	
		7 × 7	[112, 56, 28, 14]	5.81	2.75	2.63	576	<b>78.24</b>	
		$\square$ 7 × 7 <sup>⊗</sup>	[112, 56, 28, 14]	5.76	2.70	-	636	77.91	
$\square$ 7 × 7 <sup>⊖</sup>	[112, 56, 28, 14]	5.43	2.64	2.33	788	76.83			

training protocol from previous works [32, 34] using the Semantic FPN framework [26]. As illustrated in Table 4, RecNeXt demonstrates favorable mIoU-latency trade-offs across various model sizes, with RecNeXt-M3 achieving the highest mIoU of 41.0% among other models of similar scale. RecNeXt-M4 and RecNeXt-M5 also achieve competitive mIoU and latency compared to the state-of-the-art models. These findings emphasize the critical role of efficient backbones with large receptive fields in advancing semantic segmentation, especially in computationally constrained environments.

### 4.3. Ablation Studies

We systematically investigate the impact of convolutional kernel sizes, recursive decomposition, upsampling operations, and RecConv variants on model performance across different image resolutions. Experiments were conducted over 120 epochs on ImageNet-1K [8] using RecNeXt-M1 as the baseline, at resolutions of 224 × 224 and 384 × 384.

**Kernel size.** Increasing convolution kernel sizes significantly enhance model performance, especially for higher-resolution images. As shown in Table 5, expanding the kernel from 3 × 3 to 7 × 7 for 224 × 224 images boosts top-1 accuracy from 74.64% to 75.52% (+0.88%). However, this increase comes with a rise in parameter count from 4.80M to 4.96M and a slight increase in latency from 1.24ms to 1.27ms. Further enlarging the kernel to 11 × 11 slightly reduces accuracy to 75.41%, while increasing parameters to 5.26M and rising latency to 1.31ms. For 384 × 384 images, kernel enlargement delivers consistent accuracy im-

provements, achieving a +1.65% enhancement (76.35% → 78.00%) as the kernel grows from 3 × 3 to 11 × 11, with a modest latency increase (+0.20ms). These findings reveal a trade-off between the computational efficiency of smaller convolution kernels and the enhanced spatial feature capture of larger convolution kernels.

**Recursive decomposition.** The integration of recursive decomposition expands the model’s receptive field (7→80) and improves multi-scale feature aggregation, leading to accuracy gains across resolutions. For 224 × 224 images, decomposition with 5 × 5 kernels achieves a top-1 accuracy of 76.03%, outperforming single-level configurations with larger kernel sizes of 7 × 7 (75.52%) and 11 × 11 (75.41%). The benefits are even more pronounced for larger image resolutions (384 × 384), where the peak top-1 accuracy of 78.11% is achieved compared to 77.42%, without substantial changes in parameter count or FLOPs. However, the method increases latency (2.2ms → 2.8ms) and significantly reduces throughput (1200 img/s → 300 img/s). This partially due to the extensive employment of bilinear up-sampling operation, which can be replaced by a transposed depthwise convolution for improved performance, albeit at the cost of increased computational complexity. In summary, the progressive decomposition allows the network to effectively aggregate multi-frequency representations while balancing computational complexity by distributing operations across different spatial scales.

**Upsampling operation.** Table 5 demonstrates the effectiveness of substituting bilinear upsampling with transposed depthwise convolution for 384 × 384 images, While

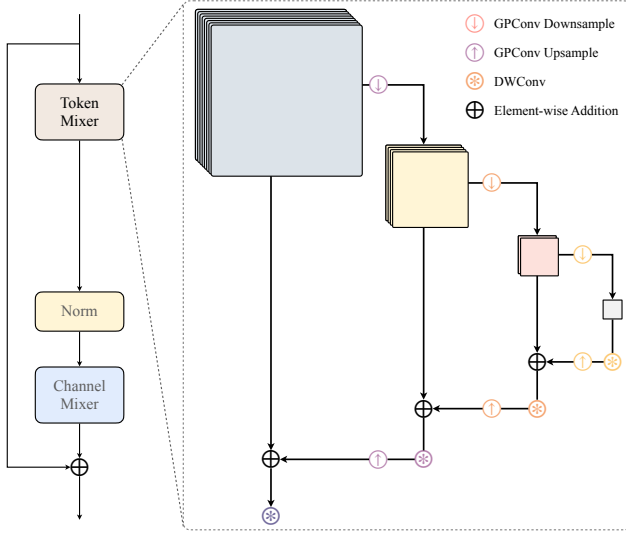


Figure 3. **RecConv Variant A.** Recursive decomposition is implemented along both spatial and channel dimensions simultaneously. The shared downsample operation is replaced with group convolutions, where the number of groups matches the number of output channels. Bilinear upsample operations are substituted with transposed group convolutions, where the number of groups corresponds to the number of input channels.

this replacement slightly increases computational complexity and parameter count, it potentially enhances feature fidelity during upsampling, resulting in a modest increase in top-1 accuracy from 78.03% to 78.24% with  $7 \times 7$  kernels. Additionally, it reduces latency from 2.84ms to 2.63ms and boosts throughput from 300img/s to 580img/s. However, smaller kernel sizes (e.g.,  $5 \times 5$  and  $3 \times 3$ ) lead to performance degradation, with accuracy dropping from 78.11% to 77.87% and from 77.72% to 77.26%, respectively.

**RecConv Variants.** We present two RecConv variants (Figure 3 and 4) incorporating recursive decomposition along both spatial and channel dimensions. These variants improve computational efficiency but at the cost of accuracy. As summarized in Table 5, the variant in Figure 3 reduces parameter from 5.81M to 5.76M, FLOPs from 2.75G to 2.70G, and increases throughput from 576img/s to 636img/s, but results in a 0.33% drop in accuracy (from 78.24% to 77.91%). Meanwhile, the latency increases significantly due to the lack of adaptation of the transposed group convolution on the NPU. The variant in Figure 4 further reduces parameters by 0.4M and FLOPs by 0.1G, lowers latency by 0.3ms, and increases throughput by 200 img/s, but causes a more significant accuracy drop of 1.4%. This comparative analysis highlights the trade-off between upsampling strategies and decomposition methods in optimizing performance and computational efficiency. This study emphasizes design simplicity, using parameter-free bilinear upsampling operation and spatial-only decomposition to achieve a balanced solution.

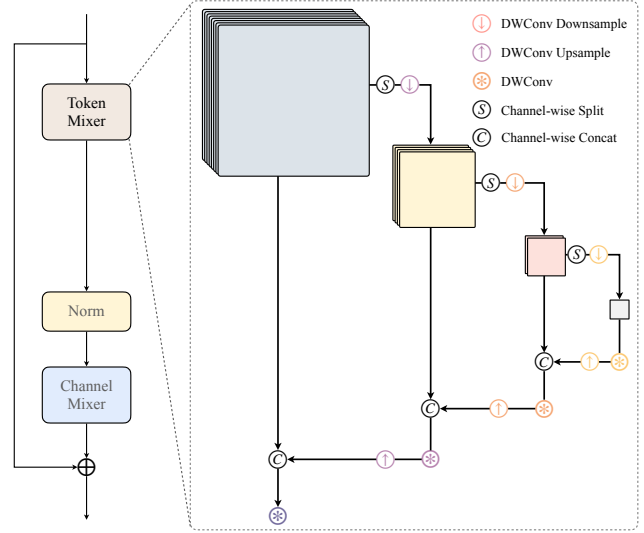


Figure 4. **RecConv Variant B.** The recursive decomposition operation is jointly performed in both spatial and channel dimensions. The shared downsample operation is replaced with channel-wise split operations, followed by depthwise convolutions. Bilinear upsample operations are converted to transposed depthwise convolutions, and element-wise addition is substituted with channel-wise concatenation.

## 5. Conclusions

This paper introduces a straightforward and versatile recursive decomposition strategy that leverages small-kernel convolutions to construct multi-frequency representations, establishing a linear relationship between parameter growth and decomposition levels. This innovation guarantees that the computational complexity at each decomposition level follows a geometric progression, diminishing exponentially with increasing depth. This recursive design is compatible with various operations and can be extended to other modalities, though this study focuses on vision tasks using basic functions. Leveraging this approach, we construct RecConv as a plug-and-play module that can be seamlessly integrated into existing computer vision architectures. To the best of our knowledge, this is the first effective convolution kernel up to  $80 \times 80$  for resource-constrained vision tasks. Building on RecConv, we introduce RecNeXt, an efficient large-kernel vision backbone optimized towards resource-constrained scenarios. Extensive experiments across multiple vision benchmarks demonstrate RecNeXt’s superiority over current leading approaches without relying on structural reparameterization or neural architecture search.

*Limitations:* While RecNeXt delivers competitive performance, its scalability lags behind the state-of-the-art models without knowledge distillation, where larger variants experience performance saturation and increased latency. Additionally, RecNeXt exhibits the lowest throughput among models of comparable parameter size due to the computational overhead of bilinear



interpolation, which can be mitigated by employing transposed convolution. The recursive decomposition may introduce numerical instability during mixed precision training, which can be alleviated by using fixed-point or BFloat16 arithmetic. Compatibility issues with bilinear interpolation and transposed convolution on certain iOS versions may also result in performance degradation.

## References

- [1] Core ml tools. <https://github.com/apple/coremltools>, 2021. 5
- [2] Nicolas Carion, Francisco Massa, Gabriel Synnaeve, Nicolas Usunier, Alexander Kirillov, and Sergey Zagoruyko. End-to-end object detection with transformers. In *European conference on computer vision*, pages 213–229. Springer, 2020. 1
- [3] Honghao Chen, Xiangxiang Chu, Yongjian Ren, Xin Zhao, and Kaiqi Huang. Pelk: Parameter-efficient large kernel convnets with peripheral convolution. *arXiv preprint arXiv:2403.07589*, 2024. 1, 2
- [4] Jierun Chen, Shiu-hong Kao, Hao He, Weipeng Zhuo, Song Wen, Chul-Ho Lee, and S-H Gary Chan. Run, don't walk: Chasing higher flops for faster neural networks. In *Proceedings of the IEEE/CVF Conference on Computer Vision and Pattern Recognition*, pages 12021–12031, 2023. 2
- [5] Yunpeng Chen, Haoqi Fan, Bing Xu, Zhicheng Yan, Yanis Kalantidis, Marcus Rohrbach, Shuicheng Yan, and Jiashi Feng. Drop an octave: Reducing spatial redundancy in convolutional neural networks with octave convolution. In *Proceedings of the IEEE/CVF international conference on computer vision*, pages 3435–3444, 2019. 2
- [6] Yinpeng Chen, Xiyang Dai, Dongdong Chen, Mengchen Liu, Xiaoyi Dong, Lu Yuan, and Zicheng Liu. Mobileformer: Bridging mobilenet and transformer. In *Proceedings of the IEEE/CVF Conference on Computer Vision and Pattern Recognition*, pages 5270–5279, 2022. 2
- [7] Yukang Chen, Jianhui Liu, Xiangyu Zhang, Xiaojuan Qi, and Jiaya Jia. Largekernel3d: Scaling up kernels in 3d sparse cnns. In *Proceedings of the IEEE/CVF Conference on Computer Vision and Pattern Recognition*, pages 13488–13498, 2023. 2
- [8] Jia Deng, Wei Dong, Richard Socher, Li-Jia Li, Kai Li, and Li Fei-Fei. Imagenet: A large-scale hierarchical image database. In *2009 IEEE conference on computer vision and pattern recognition*, pages 248–255. Ieee, 2009. 5, 7
- [9] Xiaohan Ding, Xiangyu Zhang, Jungong Han, and Guiguang Ding. Scaling up your kernels to 31x31: Revisiting large kernel design in cnns. In *Proceedings of the IEEE/CVF conference on computer vision and pattern recognition*, pages 11963–11975, 2022. 1, 2
- [10] Xiaohan Ding, Yiyuan Zhang, Yixiao Ge, Sijie Zhao, Lin Song, Xiangyu Yue, and Ying Shan. Unireplknet: A universal perception large-kernel convnet for audio, video, point cloud, time-series and image recognition. *arXiv preprint arXiv:2311.15599*, 2023. 2
- [11] Luo donghao and wang xue. ModernTCN: A modern pure convolution structure for general time series analysis. In *The Twelfth International Conference on Learning Representations*, 2024. 2
- [12] Alexey Dosovitskiy, Lucas Beyer, Alexander Kolesnikov, Dirk Weissenborn, Xiaohua Zhai, Thomas Unterthiner, Mostafa Dehghani, Matthias Minderer, Georg Heigold, Sylvain Gelly, et al. An image is worth 16x16 words: Transformers for image recognition at scale. *arXiv preprint arXiv:2010.11929*, 2020. 1, 2
- [13] Shahaf E Finder, Roy Amoyal, Eran Treister, and Oren Freifeld. Wavelet convolutions for large receptive fields. In *European Conference on Computer Vision*, 2024. 2
- [14] Benjamin Graham, Alaaeldin El-Nouby, Hugo Touvron, Pierre Stock, Armand Joulin, Herve Jegou, and Matthijs Douze. Levit: A vision transformer in convnet's clothing for faster inference. In *Proceedings of the IEEE/CVF International Conference on Computer Vision (ICCV)*, pages 12259–12269, 2021. 4
- [15] Meng-Hao Guo, Cheng-Ze Lu, Qibin Hou, Zhengning Liu, Ming-Ming Cheng, and Shi-Min Hu. Segnext: Rethinking convolutional attention design for semantic segmentation. *arXiv preprint arXiv:2209.08575*, 2022. 2
- [16] Kai Han, Yunhe Wang, Qi Tian, Jianyuan Guo, Chunjing Xu, and Chang Xu. Ghostnet: More features from cheap operations. In *CVPR*, 2020. 2
- [17] Haoyang He, Jiangning Zhang, Yuxuan Cai, Hongxu Chen, Xiaobin Hu, Zhenye Gan, Yabiao Wang, Chengjie Wang, Yunsheng Wu, and Lei Xie. Mobilemamba: Lightweight multi-receptive visual mamba network. *arXiv preprint arXiv:2411.15941*, 2024. 2
- [18] Kaiming He, Xiangyu Zhang, Shaoqing Ren, and Jian Sun. Deep residual learning for image recognition. In *Proceedings of the IEEE conference on computer vision and pattern recognition*, pages 770–778, 2016. 1, 3, 6
- [19] Kaiming He, Georgia Gkioxari, Piotr Dollár, and Ross Girshick. Mask r-cnn. In *Proceedings of the IEEE international conference on computer vision*, pages 2961–2969, 2017. 6
- [20] Dan Hendrycks and Kevin Gimpel. Gaussian error linear units (gelu). *arXiv preprint arXiv:1606.08415*, 2016. 3
- [21] Andrew Howard, Mark Sandler, Grace Chu, Liang-Chieh Chen, Bo Chen, Mingxing Tan, Weijun Wang, Yukun Zhu, Ruoming Pang, Vijay Vasudevan, et al. Searching for mobilenet3. In *Proceedings of the IEEE/CVF international conference on computer vision*, pages 1314–1324, 2019. 2
- [22] Andrew G Howard, Menglong Zhu, Bo Chen, Dmitry Kalenichenko, Weijun Wang, Tobias Weyand, Marco Andreetto, and Hartwig Adam. Mobilenets: Efficient convolutional neural networks for mobile vision applications. *arXiv preprint arXiv:1704.04861*, 2017. 2
- [23] Tao Huang, Lang Huang, Shan You, Fei Wang, Chen Qian, and Chang Xu. Lightvit: Towards light-weight convolution-free vision transformers. *arXiv preprint arXiv:2207.05557*, 2022. 2
- [24] Tianjin Huang, Lu Yin, Zhenyu Zhang, Li Shen, Meng Fang, Mykola Pechenizkiy, Zhangyang Wang, and Shiwei Liu. Are large kernels better teachers than transformers for convnets?. 2023. 1

- [25] Sergey Ioffe and Christian Szegedy. Batch normalization: Accelerating deep network training by reducing internal covariate shift. In *International conference on machine learning*, pages 448–456. pmlr, 2015. 3
- [26] Alexander Kirillov, Ross Girshick, Kaiming He, and Piotr Dollár. Panoptic feature pyramid networks. In *Proceedings of the IEEE/CVF conference on computer vision and pattern recognition*, pages 6399–6408, 2019. 7
- [27] Alex Krizhevsky, Ilya Sutskever, and Geoffrey E Hinton. Imagenet classification with deep convolutional neural networks. In *Advances in neural information processing systems*, pages 1097–1105, 2012. 1, 2
- [28] Yann LeCun, Bernhard Boser, John S Denker, Donnie Henderson, Richard E Howard, Wayne Hubbard, and Lawrence D Jackel. Backpropagation applied to handwritten zip code recognition. *Neural computation*, 1(4):541–551, 1989. 1
- [29] Hao Li, Zheng Xu, Gavin Taylor, Christoph Studer, and Tom Goldstein. Visualizing the loss landscape of neural nets. In *Neural Information Processing Systems*, 2018. 3
- [30] Siyuan Li, Zedong Wang, Zicheng Liu, Cheng Tan, Haitao Lin, Di Wu, Zhiyuan Chen, Jiangbin Zheng, and Stan Z. Li. Moganet: Multi-order gated aggregation network. In *International Conference on Learning Representations*, 2024. 2
- [31] Xiang Li, Wenhai Wang, Xiaolin Hu, and Jian Yang. Selective kernel networks. In *CVPR*, 2019. 2
- [32] Yanyu Li, Geng Yuan, Yang Wen, Ju Hu, Georgios Evangelidis, Sergey Tulyakov, Yanzhi Wang, and Jian Ren. Efficientformer: Vision transformers at mobilenet speed. *Advances in Neural Information Processing Systems*, 35: 12934–12949, 2022. 2, 4, 5, 7
- [33] Yuxuan Li, Qibin Hou, Zhaohui Zheng, Ming-Ming Cheng, Jian Yang, and Xiang Li. Large selective kernel network for remote sensing object detection. In *Proceedings of the IEEE/CVF International Conference on Computer Vision (ICCV)*, pages 16794–16805, 2023. 2
- [34] Yanyu Li, Ju Hu, Yang Wen, Georgios Evangelidis, Kamyar Salahi, Yanzhi Wang, Sergey Tulyakov, and Jian Ren. Rethinking vision transformers for mobilenet size and speed. In *Proceedings of the IEEE international conference on computer vision*, 2023. 1, 2, 3, 4, 5, 6, 7
- [35] Tsung-Yi Lin, Michael Maire, Serge Belongie, James Hays, Pietro Perona, Deva Ramanan, Piotr Dollár, and C Lawrence Zitnick. Microsoft coco: Common objects in context. In *Computer Vision—ECCV 2014: 13th European Conference, Zurich, Switzerland, September 6–12, 2014, Proceedings, Part V 13*, pages 740–755. Springer, 2014. 5, 6
- [36] Shiwei Liu, Tianlong Chen, Xiaohan Chen, Xuxi Chen, Qiao Xiao, Boqian Wu, Tommi Kärkkäinen, Mykola Pechenizkiy, Decebal Mocanu, and Zhangyang Wang. More convnets in the 2020s: Scaling up kernels beyond 51x51 using sparsity. *arXiv preprint arXiv:2207.03620*, 2022. 1, 2
- [37] Ze Liu, Yutong Lin, Yue Cao, Han Hu, Yixuan Wei, Zheng Zhang, Stephen Lin, and Baining Guo. Swin transformer: Hierarchical vision transformer using shifted windows. In *Proceedings of the IEEE/CVF international conference on computer vision*, pages 10012–10022, 2021. 1, 2, 3
- [38] Zhuang Liu, Hanzi Mao, Chao-Yuan Wu, Christoph Feichtenhofer, Trevor Darrell, and Saining Xie. A convnet for the 2020s. In *Proceedings of the IEEE/CVF conference on computer vision and pattern recognition*, pages 11976–11986, 2022. 1, 2, 3
- [39] Xu Ma, Xiyang Dai, Yue Bai, Yizhou Wang, and Yun Fu. Rewrite the stars. In *Proceedings of the IEEE/CVF Conference on Computer Vision and Pattern Recognition*, 2024. 2
- [40] Xu Ma, Xiyang Dai, Jianwei Yang, Bin Xiao, Yinpeng Chen, Yun Fu, and Lu Yuan. Efficient modulation for vision networks. In *The Twelfth International Conference on Learning Representations*, 2024. 2
- [41] Muhammad Maaz, Abdelrahman Shaker, Hisham Cholakkal, Salman Khan, Syed Waqas Zamir, Rao Muhammad Anwer, and Fahad Shahbaz Khan. Edgenext: Efficiently amalgamated cnn-transformer architecture for mobile vision applications. In *International Workshop on Computational Aspects of Deep Learning at 17th European Conference on Computer Vision (CADL2022)*. Springer, 2022. 2
- [42] Sachin Mehta and Mohammad Rastegari. Mobilevit: lightweight, general-purpose, and mobile-friendly vision transformer. *arXiv preprint arXiv:2110.02178*, 2021. 2
- [43] Sachin Mehta and Mohammad Rastegari. Separable self-attention for mobile vision transformers. *arXiv preprint arXiv:2206.02680*, 2022. 2, 5
- [44] Mustafa Munir, William Avery, and Radu Marculescu. Mobilevit: Graph-based sparse attention for mobile vision applications. In *Proceedings of the IEEE/CVF Conference on Computer Vision and Pattern Recognition*, pages 2210–2218, 2023. 4
- [45] Junting Pan, Adrian Bulat, Fuwen Tan, Xiatian Zhu, Lukasz Dudziak, Hongsheng Li, Georgios Tzimiropoulos, and Brais Martinez. Edgevits: Competing light-weight cnns on mobile devices with vision transformers. In *European Conference on Computer Vision*, pages 294–311. Springer, 2022. 2
- [46] Chao Peng, Xiangyu Zhang, Gang Yu, Guiming Luo, and Jian Sun. Large kernel matters—improve semantic segmentation by global convolutional network. In *Proceedings of the IEEE conference on computer vision and pattern recognition*, pages 4353–4361, 2017. 2
- [47] Ilija Radosavovic, Raj Prateek Kosaraju, Ross Girshick, Kaiming He, and Piotr Dollár. Designing network design spaces. In *Proceedings of the IEEE conference on computer vision and pattern recognition*, pages 10428–10436, 2020. 5
- [48] Yongming Rao, Wenliang Zhao, Zheng Zhu, Jiwen Lu, and Jie Zhou. Global filter networks for image classification. *Advances in neural information processing systems*, 34:980–993, 2021. 2
- [49] Joseph Redmon, Santosh Divvala, Ross Girshick, and Ali Farhadi. You only look once: Unified, real-time object detection. In *Proceedings of the IEEE conference on computer vision and pattern recognition*, pages 779–788, 2016. 1, 2
- [50] Mark Sandler, Andrew Howard, Menglong Zhu, Andrey Zhmoginov, and Liang-Chieh Chen. Mobilenetv2: Inverted residuals and linear bottlenecks. In *Proceedings of the IEEE conference on computer vision and pattern recognition*, pages 4510–4520, 2018. 2

- [51] Abdelrahman Shaker, Muhammad Maaz, Hanoona Rasheed, Salman Khan, Ming-Hsuan Yang, and Fahad Shahbaz Khan. Swiftformer: Efficient additive attention for transformer-based real-time mobile vision applications. In *Proceedings of the IEEE/CVF International Conference on Computer Vision (ICCV)*, 2023. 1, 2, 4, 6
- [52] Karen Simonyan and Andrew Zisserman. Very deep convolutional networks for large-scale image recognition. *arXiv preprint arXiv:1409.1556*, 2014. 2
- [53] Christian Szegedy, Wei Liu, Yangqing Jia, Pierre Sermanet, Scott Reed, Dragomir Anguelov, Dumitru Erhan, Vincent Vanhoucke, and Andrew Rabinovich. Going deeper with convolutions. In *Proceedings of the IEEE conference on computer vision and pattern recognition*, pages 1–9, 2015. 2
- [54] Christian Szegedy, Vincent Vanhoucke, Sergey Ioffe, Jon Shlens, and Zbigniew Wojna. Rethinking the inception architecture for computer vision. In *Proceedings of the IEEE conference on computer vision and pattern recognition*, pages 2818–2826, 2016. 2
- [55] Christian Szegedy, Sergey Ioffe, Vincent Vanhoucke, and Alexander A Alemi. Inception-v4, inception-resnet and the impact of residual connections on learning. In *Thirty-first AAAI conference on artificial intelligence*, 2017. 2
- [56] Mingxing Tan and Quoc Le. Efficientnet: Rethinking model scaling for convolutional neural networks. In *International conference on machine learning*, pages 6105–6114. PMLR, 2019. 2
- [57] Mingxing Tan, Bo Chen, Ruoming Pang, Vijay Vasudevan, Mark Sandler, Andrew Howard, and Quoc V Le. Mnasnet: Platform-aware neural architecture search for mobile. In *Proceedings of the IEEE/CVF conference on computer vision and pattern recognition*, pages 2820–2828, 2019. 2
- [58] Ilya Tolstikhin, Neil Houlsby, Alexander Kolesnikov, Lucas Beyer, Xiaohua Zhai, Thomas Unterthiner, Jessica Yung, Andreas Steiner, Daniel Keysers, Jakob Uszkoreit, et al. Mlp-mixer: An all-mlp architecture for vision. *arXiv preprint arXiv:2105.01601*, 2021. 2
- [59] Asher Trockman and J Zico Kolter. Patches are all you need? *arXiv preprint arXiv:2201.09792*, 2022. 2
- [60] Pavan Kumar Anasosalu Vasu, James Gabriel, Jeff Zhu, Oncel Tuzel, and Anurag Ranjan. Fastvit: A fast hybrid vision transformer using structural reparameterization. *arXiv preprint arXiv:2303.14189*, 2023. 1, 2, 4, 5, 6
- [61] Pavan Kumar Anasosalu Vasu, James Gabriel, Jeff Zhu, Oncel Tuzel, and Anurag Ranjan. Mobileone: An improved one millisecond mobile backbone. In *Proceedings of the IEEE/CVF Conference on Computer Vision and Pattern Recognition*, pages 7907–7917, 2023. 2, 5
- [62] Ashish Vaswani, Noam Shazeer, Niki Parmar, Jakob Uszkoreit, Llion Jones, Aidan N Gomez, Łukasz Kaiser, and Illia Polosukhin. Attention is all you need. *Advances in neural information processing systems*, 30, 2017. 3
- [63] Shakti N Wadkar and Abhishek Chaurasia. Mobilevitv3: Mobile-friendly vision transformer with simple and effective fusion of local, global and input features. *arXiv preprint arXiv:2209.15159*, 2022. 2
- [64] Ao Wang, Hui Chen, Zijia Lin, Hengjun Pu, and Guiguang Ding. Repvit: Revisiting mobile cnn from vit perspective. *arXiv preprint arXiv:2307.09283*, 2023. 1, 2, 3, 4, 5, 6
- [65] Ao Wang, Hui Chen, Lihao Liu, Kai Chen, Zijia Lin, Jungong Han, and Guiguang Ding. Yolov10: Real-time end-to-end object detection. *arXiv preprint arXiv:2405.14458*, 2024. 1, 2
- [66] Wenhai Wang, Enze Xie, Xiang Li, Deng-Ping Fan, Kaitao Song, Ding Liang, Tong Lu, Ping Luo, and Ling Shao. Pyramid vision transformer: A versatile backbone for dense prediction without convolutions. In *Proceedings of the IEEE/CVF international conference on computer vision*, pages 568–578, 2021. 6
- [67] Tete Xiao, Mannat Singh, Eric Mintun, Trevor Darrell, Piotr Dollár, and Ross Girshick. Early convolutions help transformers see better. *Advances in neural information processing systems*, 34:30392–30400, 2021. 3
- [68] Weihao Yu, Mi Luo, Pan Zhou, Chenyang Si, Yichen Zhou, Xinchao Wang, Jiashi Feng, and Shuicheng Yan. Metaformer is actually what you need for vision. In *Proceedings of the IEEE/CVF conference on computer vision and pattern recognition*, pages 10819–10829, 2022. 3, 5, 6
- [69] Weihao Yu, Pan Zhou, Shuicheng Yan, and Xinchao Wang. Inceptionnext: when inception meets convnext. *arXiv preprint arXiv:2303.16900*, 2023. 2, 3
- [70] Seokju Yun and Youngmin Ro. Shvit: Single-head vision transformer with memory efficient macro design. *arXiv preprint arXiv:2401.16456*, 2024. 2
- [71] Haokui Zhang, Wenze Hu, and Xiaoyu Wang. Parc-net: Position aware circular convolution with merits from convnets and transformer. In *European Conference on Computer Vision*, 2022. 2
- [72] Mingshu Zhao, Yi Luo, and Yong Ouyang. Repnext: A fast multi-scale cnn using structural reparameterization, 2024. 1, 2, 3, 4, 5, 6
- [73] Sixiao Zheng, Jiachen Lu, Hengshuang Zhao, Xiatian Zhu, Zekun Luo, Yabiao Wang, Yanwei Fu, Jianfeng Feng, Tao Xiang, Philip H.S. Torr, and Li Zhang. Rethinking semantic segmentation from a sequence-to-sequence perspective with transformers. In *CVPR*, 2021. 1
- [74] Bolei Zhou, Hang Zhao, Xavier Puig, Sanja Fidler, Adela Barriuso, and Antonio Torralba. Scene parsing through ade20k dataset. In *Proceedings of the IEEE conference on computer vision and pattern recognition*, pages 633–641, 2017. 5, 6